Supporting Information

Dual-Mode Tunable Near-Perfect Terahertz Absorber Based on GST Micro-Cavity

LI Dong-Jing [1], CUI Chen-Yang [2,3], GUO Fan [4,*] and MIN Ping-Ping [3,*]

[1] Hangzhou Institute for Advanced Study, University of Chinese Academy of Sciences, Hangzhou 310024, China
[2] Harbin Institute of Technology, Harbin 150080, China
[3] Zhengzhou Advanced Research Institute, Harbin Institute of Technology, Zhengzhou 450000, China
[4] Suzhou Laboratory, Suzhou 215000, China
* Correspondence: MIN Ping-Ping, Email: minpp@hit.edu.cn; GUO Fan, Email: guof@szlab.ac.cn **(Corresponding author)**

Supplementary Note

S1. Model Parameters and Optimization of Cavity Layer Thicknesses

In the theoretical model, the treatment of GST thickness differs between the amorphous and crystalline states, reflecting their distinct physical properties. In the amorphous state (a-GST), GST functions as a low-loss dielectric material, and its geometric thickness contributes significantly to the total optical cavity length and therefore cannot be neglected. Conversely, in the crystalline state (c-GST), GST exhibits metal-like behavior with an extremely narrow skin depth, where electromagnetic reflection occurs primarily at the surface, rendering the thickness negligible for resonance considerations.

Accordingly, the GST thickness is explicitly set to 1 μm in the model. To maintain the overall optical path length of the cavity in the amorphous state, the bottom spacer thickness h_2 was reduced from 3 μm to 2 μm, compensating for the newly incorporated GST layer. This adjustment ensures that the total optical path length remains invariant, preserving the resonance frequency and absorptance of a-GST. In the c-GST state, electromagnetic shielding by the GST layer suppresses the influence of both h_2 and the GST thickness on the resonance; consequently, the c-GST performance is unaffected by this modification.

Subsequently, the optimization procedure for h_1 and h_2 was as follows:

1. Initial range estimation: Based on the Fabry-Pérot cavity resonance condition, with a center frequency of 7 THz ($\lambda_0 \approx$ 42.9 μm) and TOPAS refractive index of 2.35, the effective wavelength is ~18.3 μm. Half of that is ~9.2 μm. Considering the LC phase delay of the top resonator, the actual total cavity length is slightly smaller. With reference to literature and our structural dimensions, the sweep ranges were set to h_1 = 16–24 μm and h_2 = 1–4 μm, as shown in Fig S1.

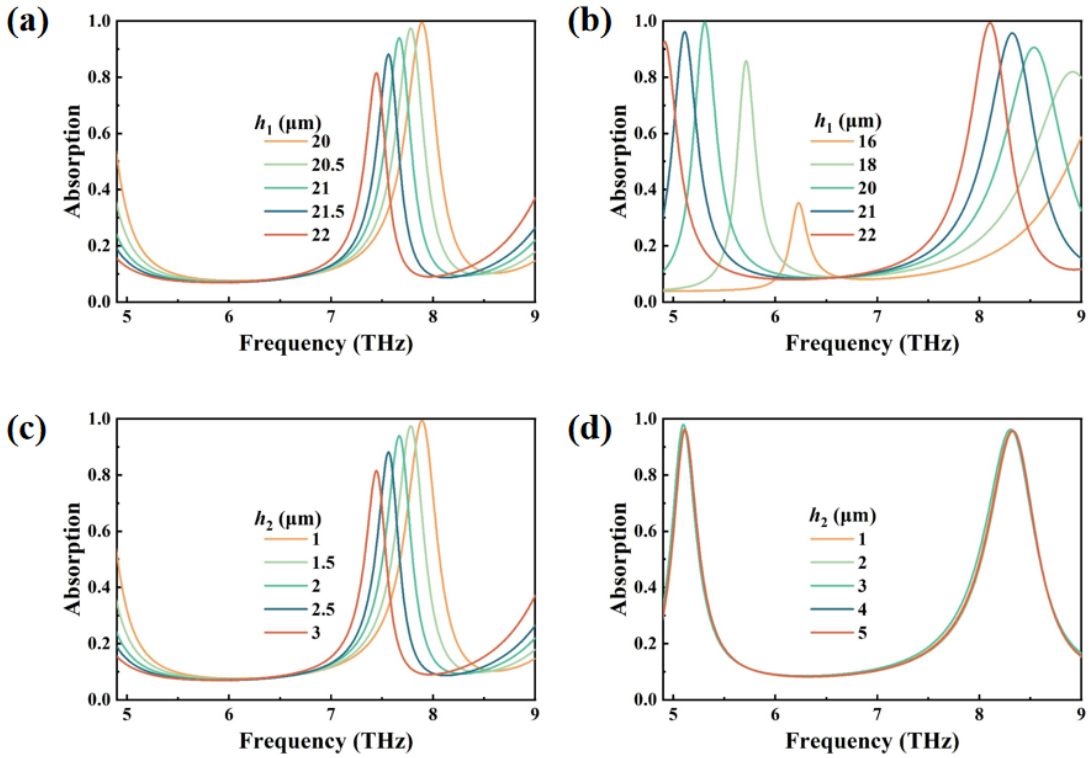


Figure S1. Optimization of cavity layer thicknesses h_1 and h_2. (a, b) Absorption spectra as a function of h_1 in the amorphous and crystalline states, respectively. (c, d) Absorption spectra as a function of h_2 in the amorphous and crystalline states, respectively.

2. Optimization strategy: Primarily optimize for the a-GST (long-cavity) state. With other geometric parameters fixed (a=1 μm, n=6 μm, m=9 μm, p=10 μm), parametric sweeps of h_1 and h_2 were performed in CST, targeting >90% absorptance at 7.7 THz for a-GST. Then the c-GST (short-cavity) state was verified: because h_2 and the GST thickness have no effect in c-GST, the dual-peak absorption depends only on h_1. For all (h_1, h_2) pairs that satisfied the a-GST requirement, the c-GST absorption spectra were calculated, requiring >90% absorptance at both 5.1 THz and 8.3 THz.
3. Optimization result: The sweep shows that with h_1 = 21 μm and h_2 = 2 μm, the requirements are satisfied: a-GST absorptance of 92% at 7.7 THz; c-GST absorptance of 91% at 5.1 THz and 93% at 8.3 THz.

S2. Theoretical Model and Calculation Procedure

The theoretical curves presented in Figures 7 and 8 of the main manuscript (showing the comparison between the theoretical model and full-wave simulations) were derived from the multiple-reflection interference model detailed in Section 5. This section provides a comprehensive description of the model framework and the step-by-step calculation procedure.

The multiple-reflection interference model treats the MIM absorber as a Fabry–Pérot cavity, in which the resonance condition is determined by the constructive and destructive interference of electromagnetic waves reflected from the cavity boundaries. By systematically calculating the phase accumulation and amplitude variations through multiple reflections, the model enables accurate prediction of the absorption spectra across different material states and structural parameters.

Procedure for obtaining the theoretical curves:

1. Model establishment: The entire MIM absorber structure is abstracted as a Fabry–Pérot cavity, consisting of a top patterned resonant layer, a bottom continuous metal reflector, and a composite dielectric layer (including GST and TOPAS spacers).
2. Calculation of the total reflection coefficient: Using the multiple-reflection interference theory, all sub-waves propagating back and forth between the top resonant layer and the bottom effective reflection interface are coherently summed, yielding the analytical expression for the total reflection coefficient r_{total} (see the formula in the original manuscript). Since the bottom metal layer thickness is much larger than the skin depth, the transmittance $T \approx 0$, and the absorptance is given by $A = 1 - |\, r_{\text{total}} \,|^2$.
3. Input material parameters: The required parameters include the complex refractive indices of all layers (GST in amorphous/crystalline states taken from literature, TOPAS with $n = 2.35$, and gold optical constants from the CST Material Library), as well as the layer thicknesses (h1 = 21 μm, h2 = 3 μm, GST layer thickness, and metal layer thickness).
4. Calculation of absorption spectra: The absorptance is calculated point by point over the frequency range of 5–9 THz using the above formula, producing the theoretical absorption curves (shown as blue hexagonal dotted lines in the figure).
5. Comparison with full-wave simulations: The theoretical results are compared with the full-wave simulation results from CST (red solid lines) to validate the model.

Key formulas:

The total reflection coefficient is:

$$r_{\text{total}} = r_{12} + \frac{t_{12} t_{21} r_{23} e^{i2\beta}}{1 - r_{21} r_{23} e^{i2\beta}}$$

The single-pass phase delay is:

$$\beta = k_0 \cdot \tilde{n}_{\text{eff}} \cdot d_{\text{eff}}$$

The GST phase transition modifies the absorption peak positions and numbers by changing the effective complex refractive index $\tilde{n}_{\text{eff}}$ and the effective cavity length d_{eff}.

S3. Polarization-Independent Absorption at Normal Incidence

The highly symmetric double-nested square-ring geometry of the absorber inherently guarantees polarization immunity under normal illumination. To explicitly verify this characteristic, additional full-wave electromagnetic simulations were performed to calculate the absorption spectra for different polarization angles (0°, 30°, 60°, 90°) in both material states.

Figure S2(a) and (b) present the absorption spectra as a function of polarization angle when GST is in the amorphous and crystalline states, respectively. At normal incidence (θ = 0°), the results demonstrate that all polarization angles yield identical absorption spectra, with perfect overlap across the entire frequency range. This confirms the polarization-independent nature of the absorber at normal incidence, which originates from the four-fold rotational symmetry of the resonant structure.

This behavior is also reflected in the main manuscript (Fig. 5), where the TE and TM polarization curves at θ = 0° completely overlap, providing implicit evidence of this symmetry property. The explicit polarization-angle scans presented here offer direct and comprehensive verification of this fundamental characteristic.

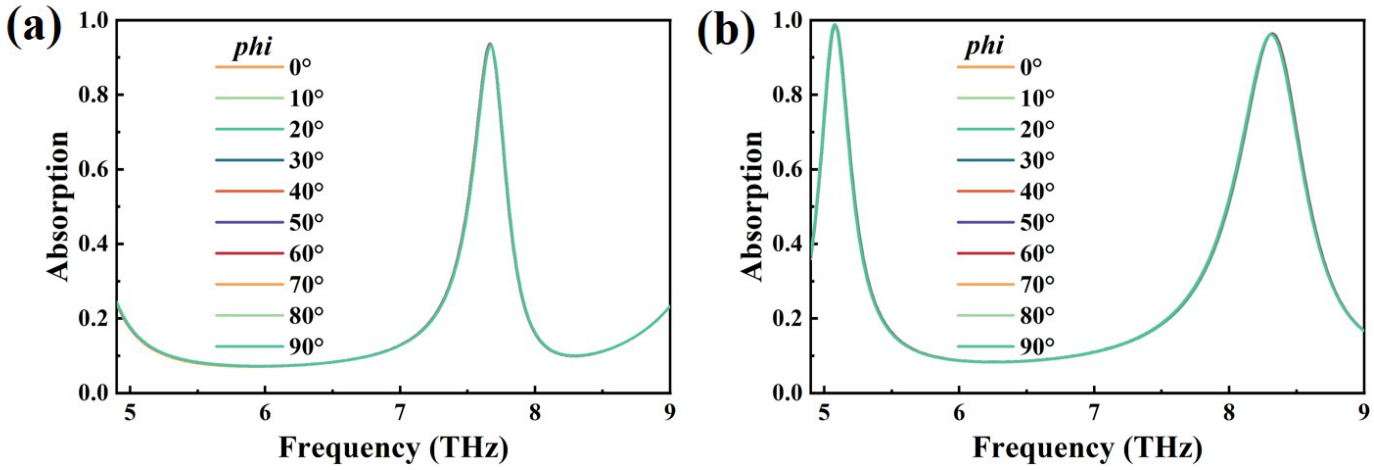


Figure S2. Polarization-independent absorption at normal incidence. (a) Absorption spectra for different polarization angles (0°, 30°, 60°, 90°) when GST is in the amorphous state (a-GST). (b) Absorption spectra for different polarization angles when GST is in the crystalline state (c-GST). The perfect overlap of all curves demonstrates the polarization-independent behavior at normal incidence ($\theta = 0°$), which is a direct consequence of the four-fold rotational symmetry of the double-nested square-ring resonator.